




Effect of Fe substitution on the partial oxidation of methane to syngas over $\text{La}_{0.7}\text{Sr}_{0.3}\text{Co}_{1-y}\text{Fe}_y\text{O}_{3-\delta}$ perovskites

Adilah ALIYATULMUNA^{1,2}, Perry BURHAN², Bambang PRIJAMBOEDI³,
Hamzah FANSURI², Irmina Kris MURWANI^{2,*}

¹Department of Chemistry, Faculty of Mathematics and Science, Universitas Negeri Malang, East Java, Indonesia

²Department of Chemistry, Faculty of Science, Institut Teknologi Sepuluh Nopember, Surabaya,
East Java, Indonesia

³Department of Inorganic and Physical Chemistry, Faculty of Mathematics and Natural Sciences,
Institut Teknologi Bandung, Bandung, Indonesia

Received: 13.11.2018

Accepted/Published Online: 18.02.2019

Final Version: 11.06.2019

Abstract: In this research, a series of $\text{La}_{0.7}\text{Sr}_{0.3}\text{Co}_{1-y}\text{Fe}_y\text{O}_{3-\delta}$ ($y = 0.0-0.4$) was successfully synthesized by a solid-state reaction method and syngas production studies were performed using gas chromatography. Thermogravimetric analysis characterized the concentration of Fe^{3+} , which gave a low H_2/CO ratio over $\text{La}_{0.7}\text{Sr}_{0.3}\text{Co}_{1-y}\text{Fe}_y\text{O}_{3-\delta}$ without the presence of molecular oxygen. All samples possessed a purely rhombohedral structure. The incorporation of more Fe increased the lattice parameter and changed XRD peaks of the $\text{La}_{1-x}\text{Sr}_x\text{Co}_{0.8}\text{Fe}_{0.2}\text{O}_3$ from sharp and single to double. Among the catalyst powders tested for syngas production activity, $\text{La}_{0.7}\text{Sr}_{0.3}\text{Co}_{0.6}\text{Fe}_{0.4}\text{O}_{3-\delta}$ ($y = 0.4$) had the low molar ratio of H_2/CO with high content of Fe^{3+} at 850 °C.

Key words: Cobalt, Fe^{3+} , H_2/CO , nonstoichiometry, solid-state reaction

1. Introduction

The research and development of syngas production technology is one of the significant efforts to produce efficient and ecofriendly energy. Nowadays, syngas is used as the raw material in clean motor vehicle synthetic fuels such as methanol, dimethyl ether, and ethanol.¹ In general, syngas is produced from natural gas, containing methane as the main component, which produces lower emission of CO_2 gas compared to the production of syngas from petroleum and coal. Thus, methane needs to be developed so that the emission of CO_2 can be eliminated or at least minimized.

Recently, the production of syngas has been widely developed through steam methane reforming (SMR). In SMR, the reaction between methane and water vapor, which produces CO and H_2 , causes the endothermic expansion of gas. However, the process of SMR tends to need a large heater to lessen the risk of explosion. Thus, a safe breakthrough or alternative innovation is needed, such as by catalytic partial oxidation (CPO). Theoretically, CPO also produces CO and H_2 , in which the reaction is exothermic, creating a lower risk of explosion compared to SMR. The most recent research shows the use of a catalyst to produce syngas by CPO using perovskite oxides, with an ABO_3 structure in which one of them is LaCoO_3 perovskite.² LaCoO_3 perovskite is not only appropriate for use as a catalyst in the production of syngas due to its content of mixed

*Correspondence: irmina@chem.its.ac.id

conductivity (ionic and electronic conductivity), but it also does not change its phase or structure during the oxidation process. The Co ion on the B site of LaCoO_3 has a high ionic and electronic conductivity, while the La ion on the A site has structural resistance to the reduction environment.³ Thus, in the present research, the material used as a catalyst in the process of methane partial oxidation to produce syngas is LaCoO_3 -based perovskite material. The substitution of two sites (A and B) from ABO_3 perovskite oxide could increase the oxygen ion transport character.

When La^{3+} was substituted by ions with a valence of $2+$, such as Ca, Sr, and Ba, the charge neutrality between the cation and oxygen anion was achieved through the oxidation of cations in the B site or oxygen ion vacancy formation. Sr was preferred to substitute parts of La in the LaCoO_3 -based perovskite over other alkaline-earth metal ions, because Sr has a higher ionic conductivity than calcium and has a greater resistance to carbonate formulation compared to calcium and barium.⁴ However, $\text{La}_{1-x}\text{Sr}_x\text{CoO}_{3-\delta}$ perovskite, as in $\text{La}_{0.3}\text{Sr}_{0.7}\text{CoO}_{3-\delta}$ or $\text{Sr}_{0.95}\text{La}_{0.05}\text{CoO}_{3-\delta}$, has the limitation of having low-structural stability in the reduction environment or under syngas formulation conditions. To increase the stability of $\text{La}_{1-x}\text{Sr}_x\text{CoO}_{3-\delta}$ perovskite, the cobalt on the B site needs to be substituted by noneasily reduced ions. Iron is the best option in this substitution because it has the highest ionic and electronic conductivity after cobalt, although it is less resistant to reducing environments than gallium, chromium, and titanium.⁵

Petric et al. found that $\text{La}_{0.7}\text{Sr}_{0.3}\text{Co}_{1-y}\text{Fe}_y\text{O}_{3-\delta}$ perovskites produce high catalytic activity.⁶ High oxygen vacancy concentration by Sr and Co on $\text{La}_{0.2}\text{Sr}_{0.8}\text{Co}_{0.8}\text{Fe}_{0.2}\text{O}_{3-\delta}$ increases the formulation of carbon and or carbonate through the reduction of CO with oxygen ion vacancies.⁷ When the A substitution in ABO_3 is studied, in this case A is La, which will be substituted by Sr. Sr substitutes as much as 30% or more ($x \geq 0.3$) of La, resulting in the formation of SrCO_3 , while the Sr substitutes less than 30% ($x < 0.3$) of La, resulting in a reduction in the amount of inner lattice oxygen in $\text{La}_{1-x}\text{Sr}_x\text{Co}_{1-y}\text{Fe}_y\text{O}_{3-\delta}$ for the catalytic oxidation of toluene.⁸ From the perspective of Fe ion to CO in $\text{La}_{1-x}\text{Sr}_x\text{Co}_{1-y}\text{Fe}_y\text{O}_{3-\delta}$, the substitution of Fe resulted in a decrease in oxygen ion vacancy concentration and a decrease in oxygen ion mobility in $\text{La}_{1-x}\text{Sr}_x\text{Co}_{1-y}\text{Fe}_y\text{O}_{3-\delta}$. However, the substitution of Fe is still needed to maintain the thermal stability of the perovskite structure. Overall, Fe substitution in limited numbers on Co can prevent a decrease in the catalytic activities of the $\text{La}_{1-x}\text{Sr}_x\text{Co}_{1-y}\text{Fe}_y\text{O}_{3-\delta}$.⁴ Thus, Fe substitution is conducted on as much as 0%, 10%, 30%, and 40% of Co ($y = 0.0-0.4$), so that the role of Co and Fe in transferring oxygen ions can be fulfilled.

No previous work investigated the role of B-site doping in $\text{La}_{0.7}\text{Sr}_{0.3}\text{Co}_{1-y}\text{Fe}_y\text{O}_{3-\delta}$ ($y = 0.0-0.4$), which was used as a catalytic agent in syngas production.⁹ A thorough study of how Fe ions affect the $\text{La}_{0.7}\text{Sr}_{0.3}\text{Co}_{1-y}\text{Fe}_y\text{O}_{3-\delta}$ material properties is required to optimize its application as a catalyst material for the partial oxidation of methane into syngas. Therefore, in the present work, $\text{La}_{0.7}\text{Sr}_{0.3}\text{Co}_{1-y}\text{Fe}_y\text{O}_{3-\delta}$ ($y = 0.0-0.4$) perovskites were investigated as catalysts for partial methane oxidation by measuring the H_2/CO ratio. Syngas (H_2 and CO) formation was then correlated through thermogravimetric analysis (TGA) of the reducibility of $\text{La}_{0.7}\text{Sr}_{0.3}\text{Co}_{1-y}\text{Fe}_y\text{O}_{3-\delta}$. Furthermore, the effects of Fe substitution in $\text{La}_{0.7}\text{Sr}_{0.3}\text{Co}_{1-y}\text{Fe}_y\text{O}_{3-\delta}$ on the crystal structure were also investigated by X-ray diffractometry (XRD).

2. Results and discussion

2.1. XRD

The XRD patterns of the $\text{La}_{0.7}\text{Sr}_{0.3}\text{Co}_{1-y}\text{Fe}_y\text{O}_{3-\delta}$ compound series in which the phase was analyzed by Match! software are shown in Figure 1. The fitting by Match! indicated that the diffraction pattern of the

$\text{La}_{0.7}\text{Sr}_{0.3}\text{Co}_{1-y}\text{Fe}_y\text{O}_{3-\delta}$ compound series matched the diffraction pattern of LaCoO_3 . The peak of the diffraction pattern at $2\theta \approx 32.8\text{--}33.2$ of $\text{La}_{0.7}\text{Sr}_{0.3}\text{Co}_{1-y}\text{Fe}_y\text{O}_{3-\delta}$ with a 40% Fe^{3+} substitution on cobalt was a double peak. Increasing the concentration of Fe would make the structure of $\text{La}_{0.7}\text{Sr}_{0.3}\text{Co}_{1-y}\text{Fe}_y\text{O}_{3-\delta}$ closer to rhombohedral. The double peak at $2\theta \approx 32.8\text{--}33.2$ is characteristic of the rhombohedral structure, which is similar to Merino et al.,¹⁰ indicating that LaCoO_3 -based perovskite is stable in the rhombohedral structure. Moreover, the structure becomes orthorhombic when the concentration of the Fe-substitute ion to Co at $\text{LaCo}_{1-y}\text{Fe}_y\text{O}_{3-\delta}$ is above 50%.

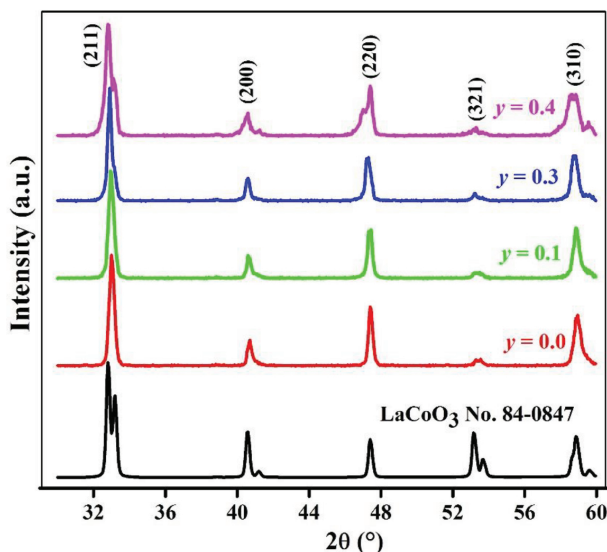


Figure 1. XRD diffraction pattern of $\text{La}_{0.7}\text{Sr}_{0.3}\text{Co}_{1-y}\text{Fe}_y\text{O}_{3-\delta}$.

By using the Rietveld method, lattice match was conducted between the $\text{La}_{0.7}\text{Sr}_{0.3}\text{Co}_{1-y}\text{Fe}_y\text{O}_{3-\delta}$ samples and the LaCoO_3 standard, corresponding to the file number PDF 84-0847 (group space R-3cR (167)); it had a rhombohedral structure. Unit cell volumes of rhombohedral symmetry were calculated with $V = a^3 \sqrt{1 - 3(\cos \alpha)^2 + 2(\cos \alpha)^3}$ where a and α are the unit cell edge length and angle between planes (crystal geometry equations for XRD: D-spacings and Miller indices). The increase in lattice parameters, that is a , and unit cell volume by Fe^{3+} ion substitute for Co ion in $\text{La}_{0.7}\text{Sr}_{0.3}\text{Co}_{1-y}\text{Fe}_y\text{O}_{3-\delta}$ was caused by the Fe ion radius, that is Fe^{3+} ($r_{\text{Fe}^{3+}} = 0.79 \text{ \AA}$) or Fe^{4+} ($r_{\text{Fe}^{4+}} = 0.72 \text{ \AA}$), which is larger compared to the Co ion radius of both Co^{4+} ($r_{\text{Co}^{4+}} = 0.67 \text{ \AA}$) and Co^{3+} ($r_{\text{Co}^{3+}} = 0.75 \text{ \AA}$). The results corresponded with the report by Hayashi et al.,¹¹ who stated that the size of the ion in the B site, in this case the Fe ion, increased the cell unit volume from LaMO_3 and NdMO_3 . The increase in Fe ions by the substitution of Co was also shown through the characteristic peaks of $\text{La}_{0.7}\text{Sr}_{0.3}\text{Co}_{1-y}\text{Fe}_y\text{O}_{3-\delta}$, shifting to a lower 2θ in Figure 2 that correlates with Bragg's law. This result was also supported by Feng,¹² who reported that the addition of a Co^{2+} ion on LaFeO_3 to form $\text{Co}_x\text{Fe}_{1-x}\text{O}_{3-\delta}$ resulted in a shift of the peak position towards a larger 2θ . The decreasing crystal sizes with Fe substitution for Co ions on $\text{La}_{0.7}\text{Sr}_{0.3}\text{Co}_{1-y}\text{Fe}_y\text{O}_{3-\delta}$ are followed by the full width at half maximum (FWHM) of the X-ray reflection at $2\theta \approx 47^\circ$ ($y = 0.0\text{--}0.4$), becoming broader in the $\text{La}_{0.7}\text{Sr}_{0.3}\text{Co}_{1-y}\text{Fe}_y\text{O}_{3-\delta}$.

The crystal size is in contrast to the FWHM value based on the formula by Scherer. The reduction in the crystal size by Fe ion substitution on Co ions at LaCoO_3 and $\text{La}_{0.6}\text{Sr}_{0.4}\text{Co}_{1-y}\text{Fe}_y\text{O}_{3-\delta}$ was individually

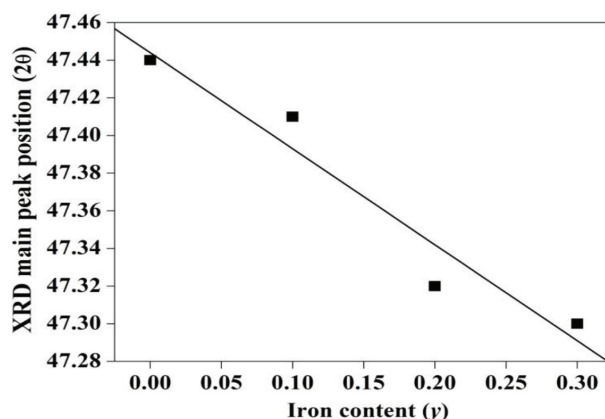


Figure 2. XRD main peak position (2θ) as a function of the iron content (y).

reported Rousseau et al.¹³ The percentage of crystallinity was obtained through the Match! software by dividing the total intensity of the peak of compound $\text{La}_{0.7}\text{Sr}_{0.3}\text{Co}_{1-y}\text{Fe}_y\text{O}_{3-\delta}$ by the total intensity of the peak of the standard compound, which was then multiplied by 100 to give a percentage. For the $\text{La}_{0.7}\text{Sr}_{0.3}\text{Co}_{1-y}\text{Fe}_y\text{O}_{3-\delta}$ compound series, the crystallinity percentage data of 99.92% ($y = 0.0$), 91.74% ($y = 0.1$), 94.86% ($y = 0.3$), and 74.99% ($y = 0.4$) were obtained. The high crystallinity of sample $y = 0.0$ ($\text{La}_{0.7}\text{Sr}_{0.3}\text{Co}_{1.0}\text{O}_{3-\delta}$) was followed by a strong intensity and a narrow peak in the same sample at $2\theta \approx 47$. The high crystallinity resulted in a sharp diffraction pattern peak; thus, FWHM became smaller, resulting in enlargement of the crystal size, as reported by Zhang,¹⁴ for the compound $\text{La}_{1-x}\text{Sr}_x\text{FeO}_{3-\delta}$.

2.2. Thermal analysis

Thermal analysis of the material obtained from the synthesis of $\text{La}_{0.7}\text{Sr}_{0.3}\text{Co}_{1-y}\text{Fe}_y\text{O}_{3-\delta}$ ($y = 0.0-0.4$) perovskite oxide was conducted through TGA and differential scanning calorimetry (DSC). The objective of this analysis was to determine the oxidation-number changes in the material-construction precursors. The results of TGA from the $\text{La}_{0.7}\text{Sr}_{0.3}\text{Co}_{1-y}\text{Fe}_y\text{O}_{3-\delta}$ oxide series ($y = 0.0-0.4$) are shown in Figure 3. The TGA curves from $\text{La}_{0.7}\text{Sr}_{0.3}\text{Co}_{1-y}\text{Fe}_y\text{O}_{3-\delta}$ are divided into four reduction zones as shown below and as reported:¹⁵

Zone I	:	$\text{Co}^{3+} \rightarrow \text{Co}^{2+}$	T = 448–570 °C
Zone II	:	$\text{Fe}^{4+} \rightarrow \text{Fe}^{3+}$	T = 563–706 °C
Zone III	:	$\text{Co}^{2+} \rightarrow \text{Co}^0$	T = 570–764 °C
Zone IV	:	$\text{Fe}^{3+} \rightarrow \text{Fe}^0$	T = 764–1100 °C

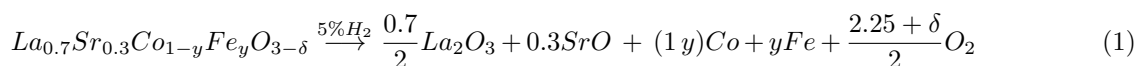
Figure 3 shows that zone I for the three compounds in the series of $\text{La}_{0.7}\text{Sr}_{0.3}\text{Co}_{1-y}\text{Fe}_y\text{O}_{3-\delta}$, which are samples $y = 0.0$, $y = 0.1$, and $y = 0.4$, does not show a different pattern in the TGA thermograms. In zone II, it can be seen that there was a mass reduction of samples $y = 0.1$ and $y = 0.4$. On the other hand, in zones II and IV, there was no mass reduction on $y = 0.0$ by Fe^{4+} ion reduction to become Fe^{3+} (zone II) or Fe^{3+} reduction to become Fe^0 (zone IV). Overall, this could happen because there is no Fe ion in sample $y = 0.0$.

In zone III, the increase in Fe-substituting ion concentration was followed by the reduction temperature from Co^{2+} becoming Co^0 , which was higher than sample $y = 0.0$ with a reduction temperature of 565 °C, followed by $y = 0.1$ at 627 °C and $y = 0.4$ at 706 °C. Furthermore, the concentration of Fe-substituting ions

also increases, resulting in a decrease in the percentage of total weight loss of 10.99%, 9.96%, and 8.02% each for samples $y = 0.0, 0.1,$ and 0.4 . This shows that the iron ion has a role in the inhibition of the reduction possibility of $\text{La}_{0.7}\text{Sr}_{0.3}\text{Co}_{1-y}\text{Fe}_y\text{O}_{3-\delta}$. Perovskite with a high iron ion concentration will be more difficult to reduce.¹⁰ The vacancy contents of oxygen ions from the $\text{La}_{0.7}\text{Sr}_{0.3}\text{Co}_{1-y}\text{Fe}_y\text{O}_{3-\delta}$ series were determined by Eq. (1); the scores are presented in the Table.

Table. Oxygen nonstoichiometry value of $\text{La}_{0.7}\text{Sr}_{0.3}\text{Co}_{1-y}\text{Fe}_y\text{O}_{3-\delta}$ in 5% hydrogen.

Sample	δ
$y = 0.0$	-0.44
$y = 0.1$	-0.22
$y = 0.4$	-0.10



Furthermore, with the iron ion substitution for cobalt in the compound series of $\text{La}_{0.7}\text{Sr}_{0.3}\text{Co}_{1-y}\text{Fe}_y\text{O}_{3-\delta}$, the oxygen ion vacancies decreased along with the iron ion substitution in cobalt. Iron ions, which are more resistant to reduction compared to cobalt ions, can resist the formulation of oxygen ion vacancies in the compound series of $\text{La}_{0.7}\text{Sr}_{0.3}\text{Co}_{1-y}\text{Fe}_y\text{O}_{3-\delta}$. Compounds with a high content of iron ions will resist reduction and produce a decrease in oxygen vacancy concentration.⁴ The sequence of the lattice oxygen ion mobility of the $\text{La}_{0.7}\text{Sr}_{0.3}\text{Co}_{1-y}\text{Fe}_y\text{O}_{3-\delta}$ compound series began from the highest to the lowest in sample $y = 0.0 > y = 0.1 > y = 0.4$. The highest ion mobility for sample $y = 0.0$ was affected by the highest oxygen ion vacancy on the same sample.¹⁶ The thermal analysis of the perovskite oxide powder $\text{La}_{0.7}\text{Sr}_{0.3}\text{Co}_{1-y}\text{Fe}_y\text{O}_{3-\delta}$ was performed through DSC, shown in Figure 4.

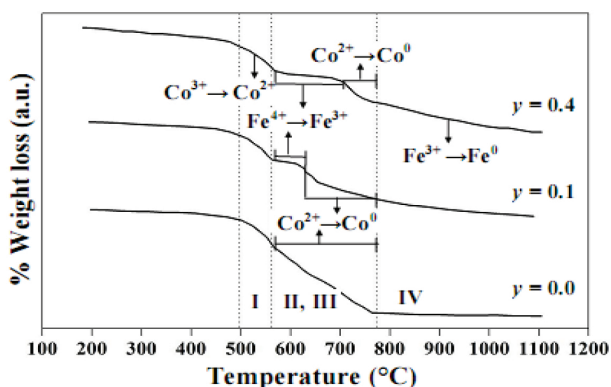


Figure 3. TGA thermogram of 5% H_2 from $\text{La}_{0.7}\text{Sr}_{0.3}\text{Co}_{1-y}\text{Fe}_y\text{O}_{3-\delta}$.

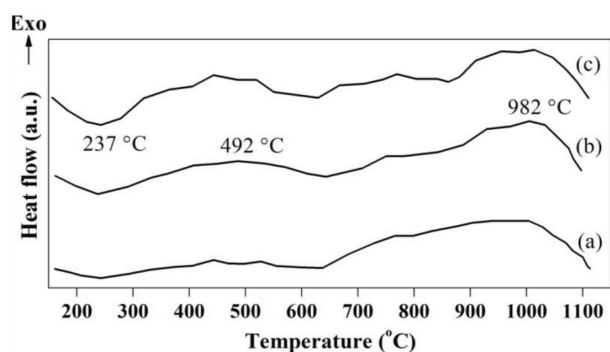


Figure 4. DSC curve of $\text{La}_{0.7}\text{Sr}_{0.3}\text{Co}_{1-y}\text{Fe}_y\text{O}_{3-\delta}$. Curve (a) $y = 0.0$, (b) $y = 0.1$, and (c) $y = 0.4$ in 5% H_2 .

The curve has an endothermic peak at 237 °C caused by H_2O desorption from $\text{La}_{0.7}\text{Sr}_{0.3}\text{Co}_{1-y}\text{Fe}_y\text{O}_{3-\delta}$, which is hygroscopic, while the peak is exothermic at 492 and 982 °C; these results were obtained from the lattice oxygen release of the compound, and are in accordance with previous observations.¹⁷ They showed that the endothermic peak is due to the loss of hydrated water present in the $\text{Ba}_{0.5}\text{Sr}_{0.5}\text{Co}_{0.8}\text{Fe}_{0.2}\text{O}_{3-\delta}$, while the exothermic peak shows a reduction reaction of $\text{Li}_{0.5}\text{CoO}_2$ and releases oxygen. In addition, for sample $y =$

0.0, the peak amplitude at 492 °C, which was small, was caused by the nonexistence of Fe ions. However, at 982 °C, it became enlarged. The peak amplitude increased with the elevation of oxygen nonstoichiometry.¹⁸

2.3. Catalytic activity tests

The $\text{La}_{0.7}\text{Sr}_{0.3}\text{Co}_{1-y}\text{Fe}_y\text{O}_{3-\delta}$ compound series was used as catalysts to produce syngas through methane partial oxidation activity. The results of the observation showed that methane conversion resulting from this series of catalysts reached approximately 90%, as shown in Figure 5. The methane conversion obtained by $\text{La}_{0.7}\text{Sr}_{0.3}\text{Co}_{1-y}\text{Fe}_y\text{O}_{3-\delta}$ increased with the reaction temperature from 750 to 950 °C. The high reaction temperature resulted in the lattice oxygen mobility on the catalyst series of $\text{La}_{0.7}\text{Sr}_{0.3}\text{Co}_{1-y}\text{Fe}_y\text{O}_{3-\delta}$ increasing; thus, the methane conversion by the catalyst $\text{La}_{0.7}\text{Sr}_{0.3}\text{Co}_{1-y}\text{Fe}_y\text{O}_{3-\delta}$ also increased, as reported previously.¹⁹ Across the whole temperature range, the methane conversion obtained with the support of the catalyst $y = 0.4$ drastically increases. This was due to oxygen nonstoichiometry of the catalyst $y = 0.4$, which was the smallest; thus, the catalyst $y = 0.4$ had the highest oxygen vacancy.

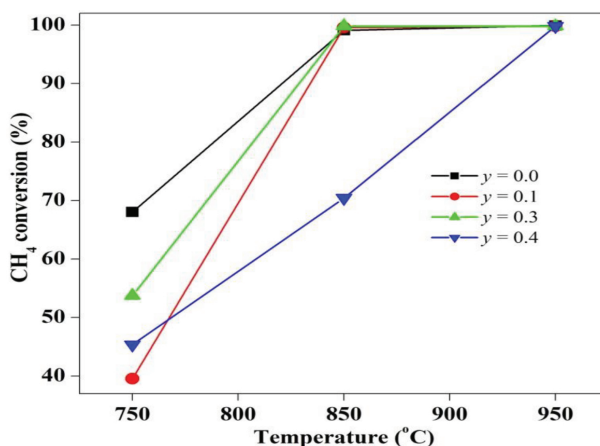


Figure 5. Methane conversion of $\text{La}_{0.7}\text{Sr}_{0.3}\text{Co}_{1-y}\text{Fe}_y\text{O}_{3-\delta}$. Reaction conditions were: feed 5% CH_4/N_2 , GHSV = $1053 \text{ mL h}^{-1} \text{ min}^{-1}$, quartz/catalyst = 2.

In the overall temperature range, the highest selectivity towards CO was observed for catalyst $y = 0.0$. This was caused by the catalyst being easy to reduce (no Fe ion content); thus, the lattice oxygen ion was easily released from the catalyst $y = 0.0$. At 950 °C, the sample range from the $\text{La}_{0.7}\text{Sr}_{0.3}\text{Co}_{1-y}\text{Fe}_y\text{O}_{3-\delta}$ series produced the highest to the lowest CO selectivity based on the iron ion concentration, which ranged from the highest to the lowest; those were samples $y = 0.4$, $y = 0.1$, and $y = 0.0$. The results of the thermogram calculation (Figure 3) showed that the concentration of the highest Fe^{3+} ion by sample was $y = 0.4$ (76.5%), followed by sample $y = 0.1$ (53%). Meanwhile, sample $y = 0.0$ did not contain Fe^{3+} . In addition, the CO selectivity produced by samples $y = 0.4$, 0.1 , and 0.0 were 11.4%, 5.6%, and 2.5%, respectively. The methane partial oxidation phenomenon using the support of catalyst $y = 0.4$ resulted in the lattice oxygen ion being released from the catalyst bulk $y = 0.4$ at 950 °C through the oxygen ion vacancies formed by the reduction of the Fe^{3+} ion to Fe^0 with ion C from the activated CH_4 .¹⁷ The lattice oxygen released through the oxygen ion vacancies of Fe^{3+} ion reduction showed that Fe^0 was the selective lattice oxygen for CO formation. Thus, at 950 °C, the CO selectivity produced by catalyst $y = 0.4$ increased. In Figure 3, it is shown that the Fe^{3+} ion reduction to Fe^0 takes place at the highest temperature, i.e. 764 to 1100 °C. The higher the temperature

needed to release the lattice oxygen through the oxygen ion vacancies of the reduction result on the B site, the more selective the lattice oxygen was at producing CO. The Fe ion reduction at the highest temperature for catalysts resulted in selective methane oxidation to produce CO.¹⁹

The ratio of H₂ to CO towards the partial oxidation of CH₄ is shown in Figure 6. Except for catalyst $y = 0.0$, at 950 °C, the sequence of H₂/CO ratio produced by the catalyst La_{0.7}Sr_{0.3}Co_{1-y}Fe_yO_{3-δ} was reversed, with the CO selectivity being produced by the same catalyst. Furthermore, at 950 °C, the low ratio of H₂/CO corresponded with the high selectivity of CO and the high content of Fe³⁺. This is in line with the findings previously reported.²⁰ The low ratio of H₂/CO (≈ 2) is appropriate when it is used as a raw material in methanol synthesis.⁵

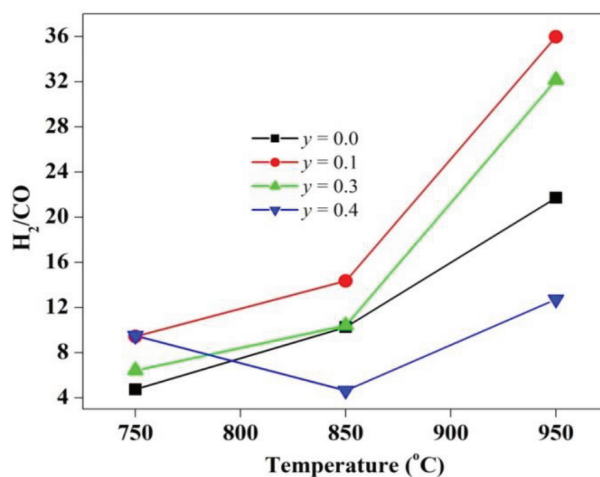


Figure 6. Ratio of H₂/CO of La_{0.7}Sr_{0.3}Co_{1-y}Fe_yO_{3-δ}. Reaction conditions were: feed 5% CH₄/N₂, GHSV = 1053 mL h⁻¹ min⁻¹, quartz/catalyst = 2.

The increase in CO₂ selectivity at 950 °C was produced by catalyst $y = 0.0$, while catalysts $y = 0.1$, $y = 0.3$, and $y = 0.4$ led to a reduction in CO₂ selectivity. The catalyst $y = 0.0$ had the highest crystallinity and the largest particle size. The large particle size resulted in a low specific surface.¹⁴ The high oxygen ion mobility and the large size of the particle for catalyst $y = 0.0$ caused CO₂ formation through the CO oxidation reaction with the lattice oxygen ion. The reduction in CO₂ selectivity produced by the catalysts $y = 0.1$, $y = 0.3$, and $y = 0.4$ was affected by the use of lattice oxygen by C atoms of activated CH₄ in the formation of CO through the methane partial oxidation reaction.

2.4. Conclusion

La_{0.7}Sr_{0.3}Co_{1-y}Fe_yO_{3-δ} ($y = 0.0, 0.1, 0.3, \text{ and } 0.4$) was successfully synthesized with a rhombohedral structure in a single phase. The structure was closer to rhombohedral when the substitution of Fe on Co of La_{0.7}Sr_{0.3}Co_{1-y}Fe_yO_{3-δ} was large. In addition, when the lattice oxygen content was larger, so was the Fe³⁺ content. When the activity of methane partial oxidation was tested, the perovskite oxide with the substitution of the highest Fe³⁺ ion was about 40% ($y = 0.4$ or La_{0.7}Sr_{0.3}Co_{0.6}Fe_{0.4}O_{3-δ}), resulting in the smallest ratio of H₂/CO, which was appropriate to produce methanol. The TGA showed the highest reduction temperature of Fe³⁺ to Fe⁰ and the perovskite powder with $y = 0.4$ contained the largest Fe³⁺ ions. From all of the oxides tested, La_{0.7}Sr_{0.3}Co_{0.6}Fe_{0.4}O_{3-δ} was the most suitable catalyst for the production of syngas.

3. Experimental

3.1. Preparation and characterization of $\text{La}_{0.7}\text{Sr}_{0.3}\text{Co}_{1-y}\text{Fe}_y\text{O}_{3-\delta}$

The perovskite material series of $\text{La}_{0.7}\text{Sr}_{0.3}\text{Co}_{1-y}\text{Fe}_y\text{O}_{3-\delta}$ ($y = 0.0\text{--}0.4$) was prepared by solid-state method and then characterized by XRD and TGA reported in a previous study for another catalyst.²¹

3.2. Catalytic activity tests

Meanwhile, catalytic tests on the reaction of methane partial oxidation through lattice oxygen from $\text{La}_{0.7}\text{Sr}_{0.3}\text{Co}_{1-y}\text{Fe}_y\text{O}_{3-\delta}$ ($y = 0.0\text{--}0.4$) were performed in a continuous reactor at atmospheric pressure and a temperature of 750, 850, and 950 °C. In every experiment, 0.5 g of catalyst powder of $\text{La}_{0.7}\text{Sr}_{0.3}\text{Co}_{1-y}\text{Fe}_y\text{O}_{3-\delta}$ perovskite oxide (0.5–0.6 mm) was mixed with quartz powder (0.5–0.6 mm) at a catalyst/quartz mass ratio of 1:2. Then the mixture of $\text{La}_{0.7}\text{Sr}_{0.3}\text{Co}_{1-y}\text{Fe}_y\text{O}_{3-\delta}$ and quartz powder was inserted inside the quartz reactor (0.4 cm diameter), which had been fitted with quartz wool at the bottom of the catalyst bed. The reactor was positioned vertically inside the furnace, with a temperature that had been kept constant through a thermocouple system. Methane gas mixed with 5% CH_4/N_2 was used as the feed gas in the partial oxidation reaction. Gas hourly space velocity (GHSV) was set at $\text{GHSV} = 1053 \text{ mL h}^{-1} \text{ min}^{-1}$ with GHSV defined as the ratio of the volumetric flow rate to the weight of catalyst in the reactor.

The resulting materials were in the form of an oxide powder of $\text{La}_{0.7}\text{Sr}_{0.3}\text{Co}_{1-y}\text{Fe}_y\text{O}_{3-\delta}$ ($y = 0.0\text{--}0.4$), from which the crystal structure was characterized by XRD, as well as for the determination of crystal size and particle crystallinity. The products of the partial oxidation reaction of methane (i.e. H_2 , CO, CO_2 , and CH_4) were analyzed quantitatively with a gas chromatograph (GC 910, produced by Buck Scientific) equipped with a TCD detector, molecular sieve of 13X columns, a Porapak Q column, and helium as carrier gas. The concentration of CH_4 , H_2 , CO, and CO_2 analyzed through GC can be used in conversion calculations of CH_4 , the selectivity on CO and CO_2 , and ratio of H_2 to CO.

Acknowledgment

The authors thank the Laboratory of Materials and Energy of the Chemistry Department, Institute of Technology Sepuluh Nopember Surabaya.

References

1. Wu, H. W.; Lin, K. W. *Int. J. Hydrogen. Energ.* **2018**, *43*, 6804-6814.
2. De Santana Santos, M.; Neto, R. C. R.; Noronha, F. B.; Bargiela, P.; da Rocha M. G. C.; Resini, C.; Carbo-Argibay, E.; Frety, R.; Bandao, S. T. *Catal. Today.* **2018**, *299*, 229-241.
3. Guo, S.; Wu, H.; Puleo, F.; Liotta, L. F. *Catalysts* **2015**, *5*, 366-391.
4. Sammells, A. F.; Mundschau, M.V. *Nonporous Inorganic Membranes: For Chemical Processing*; John Wiley & Sons: Weinheim, Germany, 2006.
5. Brandon, N. *Solid Oxide Fuel Cell Lifetime and Reliability: Critical Challenges in Fuel Cells*; Academic Press: London, United Kingdom, 2017.
6. Petric, A.; Huang, P.; Tietz, F. *Solid. State Ionics* **2000**, *135*, 719-725.
7. Scott, S. P.; Mantzavinos, D.; Hartley, A.; Sahibzada, M.; Metcalfe, I. S. *Solid State Ionics* **2002**, *152-153*, 777-781.
8. Murwani, I. K.; Scheurell, S.; Feist, M.; Kemnitz, E. *J. Therm. Anal. Calorim.* **2002**, *69*, 9-21.

9. Sunarso, J.; Hashim, S. S.; Zhu, N.; Zhou, W. *Prog. Energ. Combust.* **2017**, *61*, 57-77.
10. Merino, N. A.; Barbero, B. P.; Ruiz, P., Cadús, L. E. *J. Catal.* **2006**, *240*, 245-257.
11. Hayashi, H.; Inaba, H.; Matsuyama, M.; Lan, N. G.; Dokiya, M.; Tagawa, H. *Solid State Ionics* **1999**, *122*, 1-15.
12. Feng, C.; Ruan, S.; Li, J.; Zou, B.; Luo, J.; Chen, W.; Dong, W.; Wu, F. *Sensor. Actuat. B Chem.* **2011**, *155*, 232-238.
13. Rousseau, S.; Loridant, S.; Delichere, P.; Boreave, A.; Deloume, J. P.; Vernoux, P. *Appl. Catal. B Environ.* **2009**, *88*, 438-447.
14. Zhang, X.; Li, H.; Li, Y.; Shen, W. *Chinese J. Catal.* **2012**, *33*, 1109-1114.
15. Berry, F. J.; Gancedo, J. R.; Marco, J. F.; Ren, X. *Hyperfine. Interact.* **2005**, *166*, 449-453.
16. Castaño, M. H.; Molina, R.; Moreno, S. *Catalysts* **2015**, *5*, 905-925.
17. Patra, H.; Rout, S. K.; Pratihar, S. K.; Bhattacharya, S. *Powder. Technol.* **2011**, *209*, 98-104.
18. Cheng, X.; Wang, H.; Wei, Y.; Li, K.; Zhu, X. *J. Rare Earth.* **2010**, *28*, 316-321.
19. Xia, Y.; Sakai, T.; Fujieda, T.; Yang, X. Q.; Sun, X.; Ma, Z. F.; McBreen, J.; Yoshio, M. *J. Electrochem. Soc.* **2001**, *148*, A723-A729.
20. Li, K.; Wang, H.; Wei, Y.; Yan, D. *Appl. Catal. B Environ.* **2010**, *97*, 361-372.
21. Aliyatulmuna, A.; Utomo, W. P.; Burhan, R. Y. P.; Fansuri, H.; Murwani, I. K. *Asian. J. Chem.* **2017**, *29*, 2191-2196.